Design and Loss Analysis of Loosely Coupled Transformer for an Underwater High-Power Inductive Power Transfer System

Zhiyuan Cheng, Yang Lei, Kai Song, and Chunbo Zhu

School of Electrical Engineering and Automation, Harbin Institute of Technology, Harbin 150001, China

To prevent magnetic flux leakage to the maximal extent, increase the coupling coefficient of high-power inductive power transfer (IPT) system, and reduce the electromagnetic radiation in water medium, a novel underwater loosely coupled transformer (LCT) based on the semiclosed magnetic core structure is proposed in this paper. Power loss of the devised LCT is investigated comparatively in three media including air, freshwater, and seawater. It is shown that winding loss and core loss in the three media are basically identical. However, additional eddy current (AEC) loss in various water media is different for the sake of the difference in conductivity. In particular, AEC loss is extremely low in freshwater and relatively significant in seawater. Furthermore, when the operating frequency exceeds a certain value, AEC loss will be greater than core loss and winding loss, and become the major factor in restricting transmission efficiency of LCT in seawater. Finally, theoretical analysis and simulation are demonstrated by the underwater experiment on an IPT prototype system, which can transfer 10 kW at 91% maximal transmission efficiency and over a 25 mm air gap.

***Index Terms*— Additional eddy current (AEC) loss, loosely coupled transformer (LCT), underwater inductive power transfer (IPT), water medium.**

I. Introduction

SINCE inductive power transfer (IPT) technology realizes nonphysical connection between power and load, it overcomes many limitations of traditional power supply, such as sliding wear, contact spark, and unsafe bare conductors. In particular, it has a broad application prospect in some special cases, especially in difficult environments for the conventional power supply, e.g., mining, petrochemical smelting, flammable/explosive situations, and underwater environment [1]–[6].

The block diagram of IPT system is shown in Fig. 1. The IPT system is comprised of three parts: a loosely coupled transformer (LCT), a transmitter that provides high-frequency ac power for the primary side of LCT, and a receiver which plays a role of electrical conversion and supplies power for the load. The transmitter and receiver are independent with no mechanical connection but they keep power correlation via magnetic coupling of LCT. Meanwhile, to make up the adverse effect of leakage inductance, the primary and secondary windings usually utilize series or parallel capacitor-based resonant compensation networks to increase power transfer capability of IPT system [7], [8].

Currently, batteries are commonly used to provide power for the underwater electrical equipment, typically, such as the autonomous underwater vehicles (AUV). A contact power transfer (CPT) method is generally applied to charge the batteries. Since water is conductive, it is necessary to design a complex sealing structure to adapt to the underwater environment, e.g., serious abrasion on the interface will result in a risk of electrical leakage. Therefore, it may become a problem to charge the battery underwater by contact charging technology. However, IPT technology can accomplish power transmission using contact less connection so that the power side is completely isolated from the load side. Thus, it ensures isolation between circuit system and the underwater environment without requiring a complex and costly sealing structure. Consequently, IPT is more suitable for underwater environment than CPT. In particular, some important undersea surveys and communication tasks with the onshore facilities are completed by the undersea high-precision instruments which are highly susceptible to electromagnetic interference. Therefore, it is very important for the LCT structure design to minimize magnetic flux leakage and prevent electromagnetic radiation to the surrounding electronic and communication equipments [9]–[13].

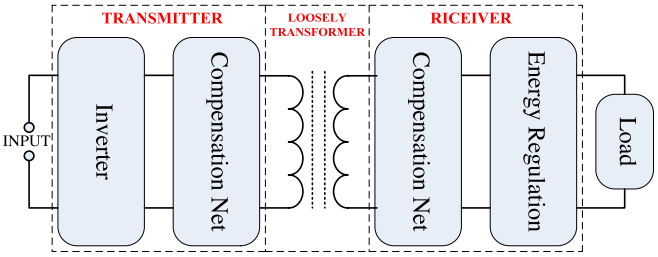

Fig. 1. Block diagram of IPT system.

In particular, there are fewer studies related to the underwater applications of IPT system. Zhou *et al.* [6] analyzed transmission efficiency and power loss of LCT in sea and air, and focused on the mutual influence between frequency, load, and additional eddy current (AEC) loss undersea. The optimal operating frequency was chosen by theoretical and experimental analysis so that maximal transmission efficiency can be achieved in IPT system. Li *et al.* [14] used reluctance model to analyze the effect on transmission performance of IPT system under high-pressure deep-sea environment and the asymmetric situation. It showed that the seawater and high pressure had a little effect on the transmission power

Manuscript received February 9, 2014; revised April 22, 2014 and July 2, 2014; accepted August 3, 2014. Date of publication August 8, 2014; date of current version June 26, 2015. Corresponding author: K. Song and C. Zhu (e-mail: kaisong@hit.edu.cn; zhuchunbo@hit.edu.cn).

Color versions of one or more of the figures in this paper are available online at http://ieeexplore.ieee.org.

Digital Object Identifier 10.1109/TMAG.2014.2346737

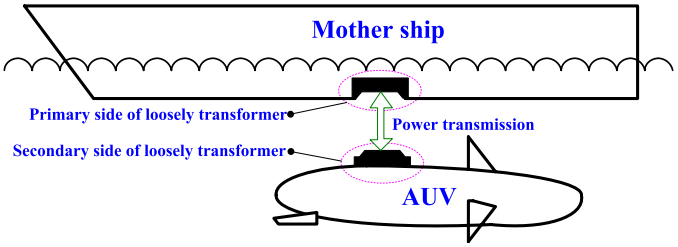

Fig. 2. General schematics of underwater IPT system.

of IPT system, while the asymmetrical operation made a great difference. Kojiya *et al*. [15] designed a novel structure of LCT suitable for AUV, optimized the winding structure and studied power transmission characteristics both in air and under seawater. Fukuda *et al*. [16] designed a structure of LCT which could transfer both power and signals for the undersea AUV. In particular, the signals and energy were transmitted in the different frequency bands, respectively.

The above literatures related to underwater applications of IPT system are mainly focused on low power (i.e., several hundreds of watts) because of technical limitations of coil size and power inverter. However, underwater appliances are currently utilizing battery pack with a high efficiency and a high-energy density, which inevitably will increase the charging current. Thus, research on an underwater high-power IPT system is important. This paper focuses on a high-power IPT system for AUV charging application. The general schematics of the underwater IPT system is shown in Fig. 2. First, a novel semiclosed structure of LCT suitable for underwater application is designed, which can reduce magnetic flux leakage and prevent electromagnetic radiation effectively. Second, the power loss of the devised LCT for different frequencies and primary exciting current in three different media (i.e., air, freshwater, and seawater) are emphatically analyzed. Finally, an underwater high-power IPT prototype system is setup to verify theoretical and simulation analysis.

II. Core Structure Design of LCT

The coupling coefficient of LCT determines the power transmission capacity of the IPT system. Due to the separation of transformer's primary and secondary side, there is a large leakage inductance which leads to a relatively low-coupling coefficient. The general expression of the coupling coefficient k is given as

$$k = \frac{M}{\sqrt{L_p L_s}} \tag{1}$$

where M is the mutual inductance of transformer, L_p and L_s are the self-inductance of primary winding and secondary winding, respectively. According to (1), coupling coefficient k is closely related to the electromagnetic structure of LCT. To reduce the effect of magnetic flux leakage to surroundings and improve the coupling coefficient effectively, it is necessary to optimize the core structure of LCT over a certain air gap [17]. This paper proposes a novel semiclosed transformer structure. To further illustrate the characteristic of the devised semiclosed transformer, a 3-D finite-element model (FEM) is established and simulation analysis is done using a contactless transformer composed of a nonplanar magnetic core. The core structures of the semiclosed and open transformers are shown in Fig. 3.

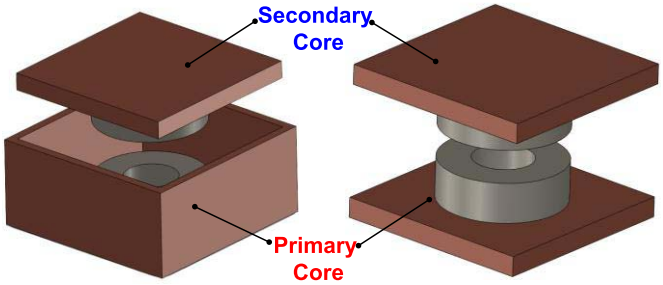

Fig. 3. Core structures of (left) semiclosed and (right) nonclosed transformers.

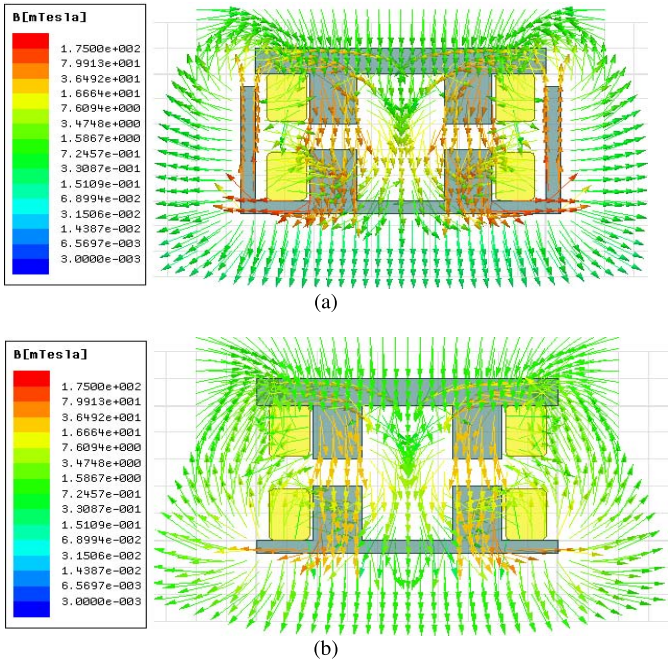

Fig. 4. Distribution of magnetic induction intensity vector in the cross-center section of LCT. The yellow part denotes the coil and the gray part denotes the core. (a) Semiclosed core structure. (b) Nonclosed core structure.

As shown in Fig. 3 (left), the core structure of the designed semiclosed LCT is not rotationally symmetric. To facilitate observation and analysis of the simulation results, a cross-center section which is parallel to the side face of LCT is employed as the research object. Fig. 4 shows the magnetic induction intensity vector in the cross-center section. Meanwhile, the simplified equivalent circuit of the transformer with an air gap of 2.5 cm between the primary and secondary winding is shown Fig. 5. Both the magnetic induction intensity vector and the eddy density distribution of the FEM are aimed at this section.

It is obvious that the secondary winding is open, while the magnetic resistance of magnetic core is negligible in Fig. 5. The coupling coefficient k can be expressed in a new form

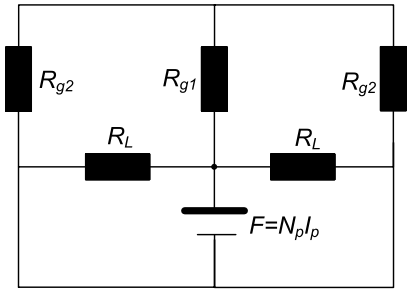

Fig. 5. Common simplified equivalent magnetic circuit of two examples of LCTs. Note that R_{g2} and R_L are different for the two examples of LCTs.

based on the magnetic equivalent circuit as

$$k = \frac{N_p I_p/(R_{g_1} + 2R_{g_2})}{N_p I_p/(R_{g_1} + 2R_{g_2}) + N_p I_p/R_L} = \frac{1}{(g_1 + 2g_2)/L + 1} \tag{2}$$

where g_1 is the distance of for the middle column, g_2 is the distance of air gap for the perimeter column in the LCT, L is the distance between the terminals of middle column and perimeter column, N_p is the number of turns, and I_p is the exciting current of primary winding. As shown in (2), the coupling coefficient k depends on g_1, g_2, and L. Note that g_2 decreases significantly while L does not vary in the semiclosed transformer. Thus, the coupling coefficient k is larger in the semiclosed transformer than the nonclosed transformer.

As shown in Fig. 4, it is obvious that most magnetic fields of the nonclosed transformer leak into the air in the position of the perimeter column, according to the color of magnetic induction intensity vector line that shows the size of magnetic induction intensity. In particular, the color inside the semiclosed magnetic core is deeper than the nonclosed one. It means that the main flux increases significantly inside the semiclosed magnetic core. Therefore, the magnetic flux leakage decreases due to the high-permeability of the ferrite core that constitutes four borders of the semiclosed transformer. Simulation results show that the coupling coefficient k between windings for the semiclosed structure grows from 0.489 to 0.548.

In summary, the semiclosed core structure is capable of inhibiting the magnetic flux leakage effectively, reducing the electromagnetic radiation, and improving the transmission efficiency of LCT in the IPT system.

III. Power Loss Analysis of LCT

LCT is a key component of IPT system. Finite-element simulation software is used for magnetic and electric circuit analysis. Kim *et al.* [18] proposed a method to reduce leakage magnetic of LCT using ferromagnetic material and metal shield. Umenei *et al.* [19] presented a method to open up a flux path from the primary to the secondary coil to achieve IPT using the nonlinearity of a ferrite flux shield. Zhang *et al.* [20] developed a 3-D finite-element method to model wireless power transfer system using displacement current and eddy current. The power loss of LCT is the main factor that influences the transmission efficiency of IPT system. For conventional applications of IPT system, power loss of the transformer mainly comprises the core loss and the winding loss [21]. Given the specificity of IPT application under water, AEC loss that will also affect the transformer efficiency in water should be analyzed besides the core loss and the winding loss. What's more, the transmission efficiency of LCT will be greatly affected in water if AEC loss is suppressed ineffectively. To investigate power loss characteristics of LCT in different media, this paper analyzes core loss, winding loss, and AEC loss of water media, comparatively.

A. Core Loss

In general, the core loss P_{Fe} [22], [23], includes magnetic hysteresis loss P_{hyst}, excess loss P_{ex}, and eddy loss P_{eddy} [24]. The expression is as follows:

$$P_{\text{Fe}} = P_{\text{hyst}} + P_{\text{ex}} + P_{\text{eddy}} = \beta_0 B_m^2 f_w + \beta_1 (B_m f_w)^{1.5} + \beta_2 B_m^2 f_w^2 \tag{3}$$

where β_0, β_1, and β_2 are parameters related to the magnetic core material, f_w is the operating frequency of the IPT system and B_m denotes the maximum of magnetic induction intensity. In general, soft magnetic material with high permeability, high-saturation magnetization, and low-hysteresis loss is a traditional choice in IPT system. It means that the material parameter β_0 is so small that the magnetic hysteresis loss is low enough to be neglected. For the convenience of analysis, assume that a magnetization process is perfectly homogeneous in space, additional loss is negligible and $\beta_1 = 0$. It is crucial that, skin effect should be considered in the eddy loss, but the skin effect is relatively small in this paper for the low-frequency IPT system. According to the classical expression of eddy loss of the soft magnetic material, the magnetic core loss of the LCT is defined as

$$P_c = \frac{\pi^2}{6}\sigma_1 h_1^2 V_1 B_{m1}^2 f_w^2 + \frac{\pi^2}{16}\sigma_1 \left(d_1^2 - d_2^2\right) V_2 B_{m2}^2 f_w^2 \tag{4}$$

where σ_1 is the conductivity of the magnetic core material, h_1 is the thickness of the planar magnetic core, d_1 and d_2 denote the inside and outside diameter of the toroidal core, respectively, V_1 and V_2 denote the volume of the planar core and the toroidal core, respectively, and B_{m1} and B_{m2} is the maximum of magnetic induction intensity of the planar core and the toroidal core, respectively. Due to the difference in the eddy distribution among the three media (i.e., air, freshwater, and seawater), magnetic field distributions of the transformer's magnetic core are different, which results in the difference of core loss. Furthermore, the simulation results show that the densities of the excitation current and the eddy current differ by orders of magnitude, while the distribution of the magnetic field in the three media is nearly constant. Conclusively, the core loss in three investigated media is basically in accordance, which coincides with the simulation results, as shown in Table I.

TABLE I
SIMULATION RESULTS OF CORE LOSS ($f_w = 40$ kHz AND $I_p = 50$ A)

Medium	Air	Freshwater	Seawater
core loss (W)	46.6099	46.7377	46.6839

TABLE II
SIMULATION RESULTS OF WINDING LOSS ($f_w = 40$ kHz AND $I_p = 50$ A)

Medium	Air	Freshwater	Seawater
winding loss (W)	294.1067	293.7923	294.3841

TABLE III
PARAMETER COMPASSION OF THREE MEDIA

Media	Relative Permittivity	Conductivity (S/m)	Relative Permeability
air	1.0006	0	1.000004
freshwater	81	0.01	0.999991
seawater	81	4	0.999991

B. Winding Loss

The winding loss is mainly composed of skin-effect loss, proximity-effect loss, and dc conduction loss [25], [26]. At present, windings of LCT in IPT system principally adopt the litz wire [27]. If diameter, turns and operating frequency of the litz wire are reasonably selected, the skin effect and the proximity effect can be reduced effectively. Thus, under the premise of disregarding the skin effect and the proximity effect, the dc conduction loss of primary winding and secondary windings can be uniquely considered as winding loss in three medium. Then, the unified expression is written as

$$P_w = I_{\text{p-rms}}^2 R_{\text{p-dc}} + I_{\text{s-rms}}^2 R_{\text{s-dc}} \tag{5}$$

where $I_{\text{p-rms}}$ and $I_{\text{s-rms}}$ is the valid value of primary and secondary current, respectively, $R_{\text{p-dc}}$ and $R_{\text{s-dc}}$ denote the dc resistance of primary and secondary winding, respectively. In addition, simulation results indicate that the winding loss in three media is basically identical, as shown in Table II.

C. Medium Loss

Table III shows the parameter comparison in three media: air, freshwater, and seawater. As shown in Table III, the relative permeability of three media is basically identical and great differences exist in the conductivity and relative permittivity, which results in the AEC loss in seawater and freshwater under the effect of alternating electromagnetic field. However, the AEC loss does not exist in air.

To further illustrate the AEC loss in different media of LCT in the IPT system, the exciting currents at the same amplitude (50 A) and frequency (20 kHz) are given to the primary winding of the LCT in the three media. Consequently,

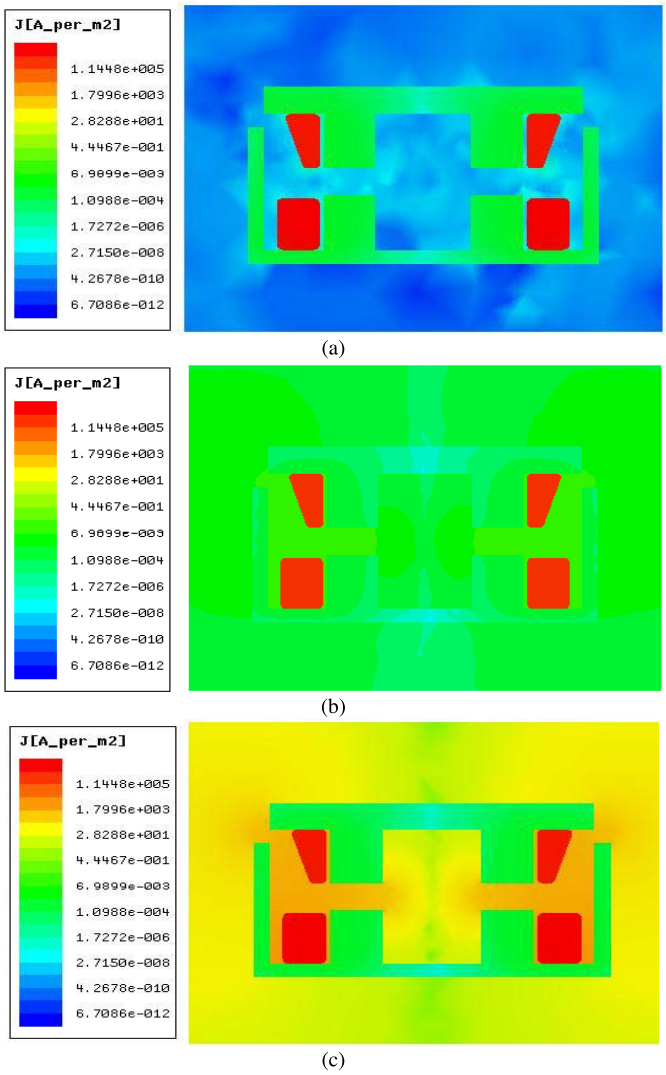

Fig. 6. Eddy current density distribution of the LCTs cross-center section in the three investigated. (a) Air medium. (b) Freshwater medium. (c) Seawater medium.

the eddy current density distributions ($\boldsymbol{J}$) of the transformer's cross-center section in the three media are as shown in Fig. 6. Obviously, the magnitude of eddy current density in freshwater is in the range of $10^{-6}-10^{-3}$ A/m^2. However, as the conductivity of seawater is relatively larger, the eddy-current density is up to $10^{1}-10^{3}$ A/m^2. Thus, the AEC loss can be ignored in freshwater since it shows a 10^9 order of magnitude difference between seawater and freshwater.

To analyze the main factors affecting the AEC loss in seawater, the paper gives an expression of the eddy-current loss in seawater caused by the exciting current

$$P_{\text{aec}} = \frac{\iiint_V |J_E|^2 \, dV}{\sigma_2} \tag{6}$$

where J_E denotes the eddy-current density in seawater, σ_2 denotes the conductivity of seawater, and V is the studied seawater area. In (6), the value of AEC loss is determined by eddy-current density and conductivity of the seawater.

For the convenience of analysis, the AEC loss excited by N-turns winding can be expressed using the cylindrical coordinate $(r-z)$ as

$$P_{\text{aec}} = \frac{2\pi N}{\sigma_2}\int_0^{\infty}\int_0^{D}|\sigma_2 E(r,z)|^2 dr dz \tag{7}$$

where $E(r,z)$ denotes the electric field intensity in seawater. Without considering the displacement current, $E(r,z)$ can be derived by the Maxwell's equations in [6] and expressed as

$$E(r,z) = j2\pi f_w \mu_2 r_0 I_p \int_0^{+\infty} J_p(\gamma r_0) \times J_p(\gamma r)(\tau_1 e^{\lambda z} + \tau_2 e^{-\lambda z}) d\gamma \tag{8}$$

where μ_2 is the permeability of seawater, r_0 is the location of exciting current, J_p denotes the exciting current density of primary winding, γ is the parameter that divides one partial differential equation into two ordinary differential equations, τ_1, τ_2, and λ are the parameters related to μ_2, σ_2, and γ. In (8), except f_w, I_p, and J_p, other parameters are just associated with the inherent attribute of seawater and the structure parameters of LCT. Therefore, in the case of the fixed exciting current, the electric field intensity in seawater is proportional to the operating frequency f_w, namely, the AEC loss is directly proportional to f_w^2.

IV. Simulation Analysis of Loose Characteristics in Three Media

On the basis of the above theoretical analysis, the most significant difference of power loss of LCT in the three media is that the AEC loss in seawater closely relates to the operating frequency and exciting current. Here, frequency and current characteristic of each loss in the three media are analyzed using the finite-element simulation software (Ansoft Maxwell).

A. Current Characteristics

Fig. 7 shows the trend of each calculated of LCT as a function of the primary excitation current change at the operating frequency of 20 kHz. Simulation results demonstrate that, by changing primary currents, the curves of winding loss and core loss in air and freshwater are basically those in seawater. Therefore, only the loss of LCT in seawater will be analyzed. Accordingly, with the exciting current increasing, all losses grow nonlinearly. In particular, the increasing trend of winding loss is the most remarkable. Increasing trend of the AEC loss is also obvious while the core loss increases slowly. Furthermore, among the three losses, the winding loss is always the highest and the AEC loss takes the second place in the total losses. As shown in Fig. 7, when the exciting current value is 100 A, the winding loss increases to kilowatt level and the AEC loss also increases to 360 W (the rated power of simulation is 40 kW). Therefore, the winding loss and the AEC loss should be mainly considered when the IPT system operates at a large primary exciting current in seawater.

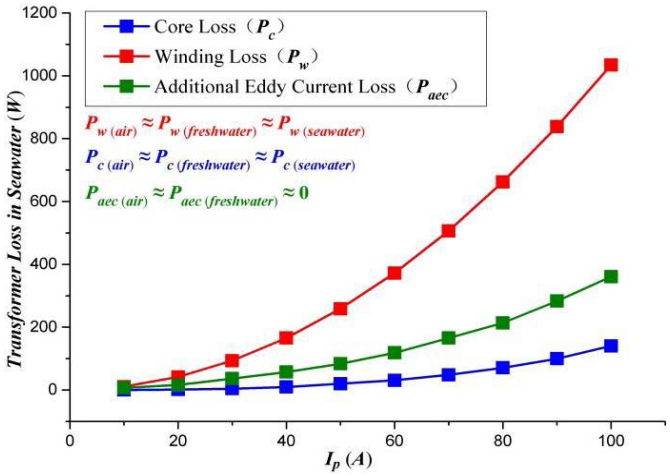

Fig. 7. Current characteristic curves of LCTs losses in three media ($f_w = 20$ kHz).

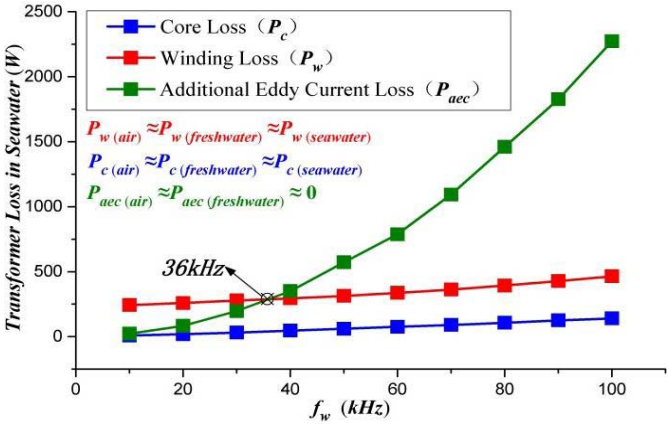

Fig. 8. Frequency characteristic curves of LCTs losses in three media ($I_p = 50$ A).

B. Frequency Characteristics

Fig. 8 shows the trend of each loss of LCT with the changed operating frequency at the primary excitation current of 50 A. Simulation results show that, with the changed operating frequency, the curves of winding loss and core loss in air and freshwater are basically in agreement with the situation in seawater. Therefore, only the loss of LCT in seawater will be analyzed. Accordingly, with the operating frequency increasing, all losses grow nonlinearly. In particular, the AEC loss has the most rapid rise, and has quadratic frequency dependence.

As follows from the theoretical analysis, the change of the winding loss with the frequency is slowly rising because it compensates the influence of the skin effect. Meanwhile, the winding loss is the main loss of LCT at a low-operating frequency. In addition, the winding loss is greater than the other two types of loss when the frequency is below 30 kHz. However, when the operating frequency exceeds a certain value (about 36 kHz), the AEC loss will exceed the winding loss and gradually become the main factor that impacts the transmission efficiency of LCT.

TABLE IV
SIMULATION PARAMETERS OF LCT

Parameters	Value
core relative permeability μ_1	3000
core conductivity σ_1	0.5 S/m
primary turns N_p	18
secondary turns N_s	17
air gap h	25mm
primary current I_p	10A~100A
operating frequency f_w	10kHz~100kHz

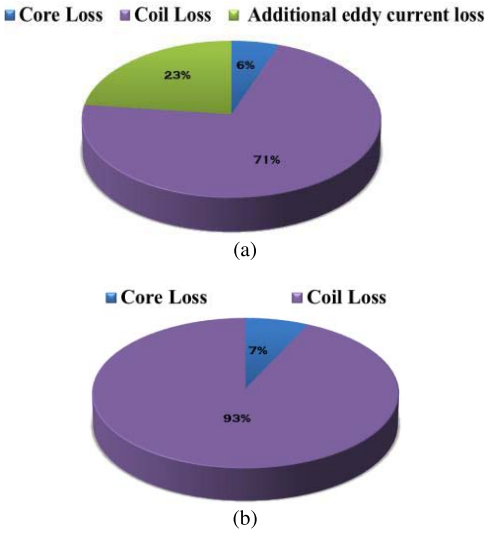

Fig. 9. Pie chart of the LCTs loss distributions in three media ($I_p = 50$ A and $f_w = 20$ kHz). (a) Seawater. (b) Air/freshwater.

Through the simulation results, the value of AEC loss can reach 2.3 kW at the operating frequency of 100 kHz. To suppress the adverse effect to transmission efficiency from the AEC loss, it is suggested that the IPT system operates at a low frequency.

C. Low-Frequency Loss Characteristics

In this paper, Mn–Zn ferrite is used in the simulation as the core material. The simulation parameters are shown in Table IV. Fig. 9 shows a pie chart of the LCTs loss distributions in air, freshwater, and seawater. Fig. 9 uses the data of Table IV to determine the primary excitation current of 50 A and the operating frequency of 20 kHz. As shown in Fig. 9, the winding loss accounts for the largest proportion of the total losses in air and freshwater, while the core loss that only contributes 7% is the lowest. In seawater, although the winding loss is still the main loss of LCT, the AEC loss which makes up about a quarter of the total losses cannot be ignored. Furthermore it explains the loss characteristics of the LCT in a low-frequency IPT system in seawater.

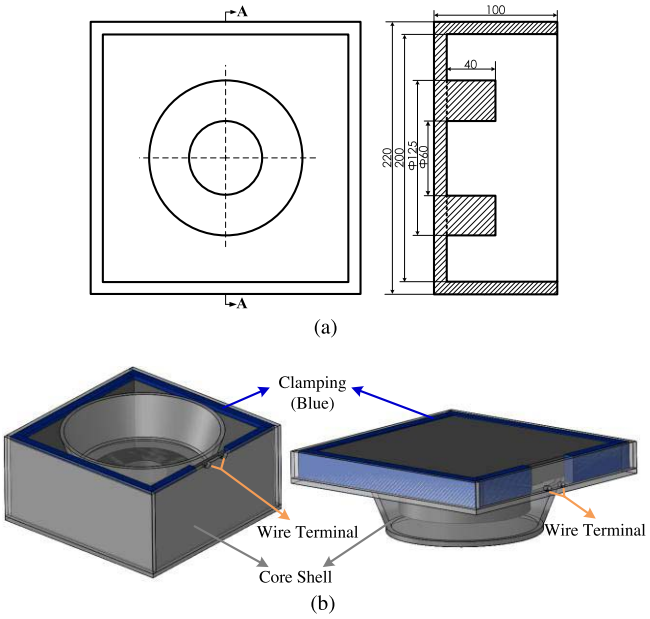

Fig. 10. Schematic diagram of the devised LCT. (a) Mechanical structure of primary core. (b) 3-D structure of the LCTs shell.

TABLE V
PARAMETERS OF THE DEVISED LCT

Parameters	Value	Unit
primary inductance L_p	250	μH
secondary inductance L_s	202	μH
mutual inductance M	106	μH
coupling coefficient k	0.47	
primary turns N_p	18	
secondary turns N_s	17	
primary winding resistance R_p (40 kHz)	0.155	Ω
secondary winding resistance R_s (40 kHz)	0.147	Ω

V. EXPERIMENTAL RESULTS AND DISCUSSION

Fig. 10(a) shows the mechanical structure of the primary core of LCT. The secondary core is obtained by removing the primary core's four sides. Both the primary core and the secondary core are made of Mn–Zn ferrite material, which has a relative permeability of 3000 ± 20%. To meet the requirements of LCT on alignment and the maximal joint degree in the experiment, a core shell is designed for the primary and second sides of LCT, by the 3-D software Solidworks combined with the shape features of the devised semiclosed core structure [Fig. 3 (left)]. In particular, a certain space is reserved in the internal part of the shell to place the wire terminal of the winding. Moreover, to avoid the mechanical shift between the primary and second sides of LCT, a clamping is placed in the shell, as shown in Fig. 10(b). Both the clamping and the shell are made of nonconductive and nonmagnetic plexiglass, which does not generate extra losses in the experiment. The detailed parameters of the devised LCT are shown in Table V.

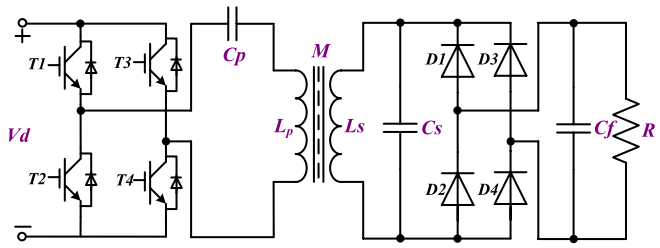

Fig. 11. Circuit structure diagram of IPT system.

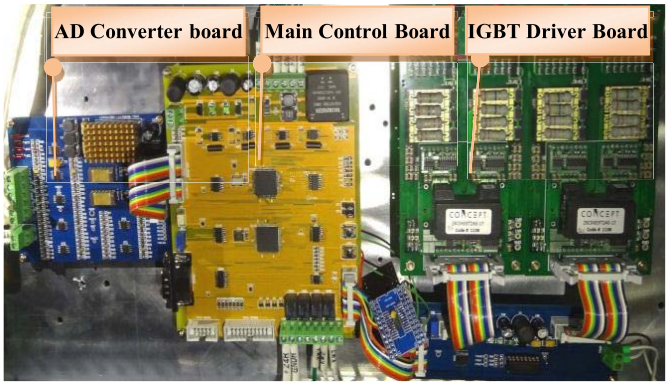

Fig. 12. Main control board of IPT system.

As shown in Fig. 11, the IPT system mainly consists of three parts: primary side inverter, resonant compensation networks, and secondary side rectifier. The primary side uses four FF150R12KF4 insulated gate bipolar transistors (IGBTs) (1200 V and 150 A) as an H-bridge inverter. The four IGBTs are controlled by four pulse modulation (PWM) signals obtained from the micro control unit (MCU) of the main control board. The primary side circuit outputs an ac voltage with an adjustable frequency, acting as a high-frequency inverter. The secondary side utilizes the uncontrolled rectifier circuit and the filter circuit to supply power for load. In this paper, the load is set to 26 Ω. In terms of the resonant compensation networks, the primary side adopts the serial resonant structure and the secondary side uses the parallel structure, respectively. Here, the high-frequency high-voltage metalized-film capacitors are used as the compensation capacitors. The structure of the main control board of the IPT system is shown in Fig. 12 and the underwater experimental photograph of the IPT system are shown in Fig. 13.

As shown in Fig. 12, the data acquisition process for resonant current and terminal voltage of resonant capacitor in the primary side is achieved by the analog-to-digital converter board. The main control board consists of a MCU (ARM STM32VET6) and a complex programmable logic device (CPLD) (Altera MAX II EPM240T100C5). MCU is used to generate PWM signals with adjustable frequencies, communicate with touch-screen in real time, control time sequence during power-on period for electrical part, and handle accident faults. CPLD is responsible for detecting fault signals that include overcurrent signal of primary resonant current, overvoltage signal of primary resonant capacitor as well as short circuit, and overcurrent and overvoltage signals in

Fig. 13. Underwater experimental photograph of IPT system.

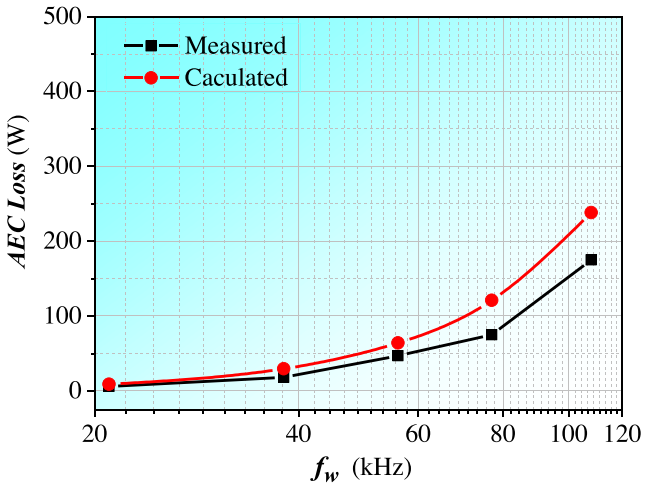

Fig. 14. Comparison of measured and calculated AEC losses at different frequencies in seawater.

IGBT module. It is capable of obtaining phase information, too. IGBT driver board has the function of driving IGBT module and outputting faults.

To increase the effect of AEC loss in the experiment, a certain amount of space between the primary and secondary shell is reserved, which results in the increased volume of seawater between the primary and secondary side. It is difficult to measure the AEC loss directly in the experiment though AEC loss is an important factor for transmission efficiency of LCT in seawater. In general, an indirect estimation method is used to measure the AEC loss [6]. Winding loss and core loss are approximately identical in seawater and air for the same primary current of LCT in the two media, namely, $\boldsymbol{P}_{w(\text{seawater})} \approx \boldsymbol{P}_{w(\text{air})}$ and $\boldsymbol{P}_{c(\text{seawater})} \approx \boldsymbol{P}_{c(\text{air})}$. Thus, the difference between the total losses of LCT in seawater and that in air is approximately the AEC loss.

The measured AEC loss at different frequencies is obtained by the above estimation method when the primary current of LCT is 10 A. Comparison of the measured and calculated losses is shown in Fig. 14. It can be seen that the trend of

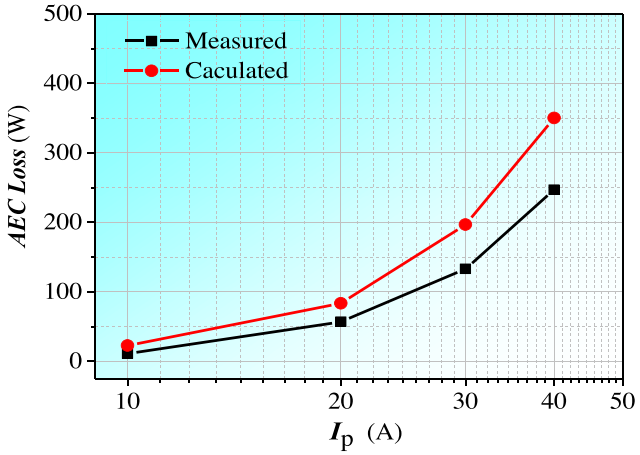

Fig. 15. Comparison of measured and calculated AEC losses at different primary currents in seawater.

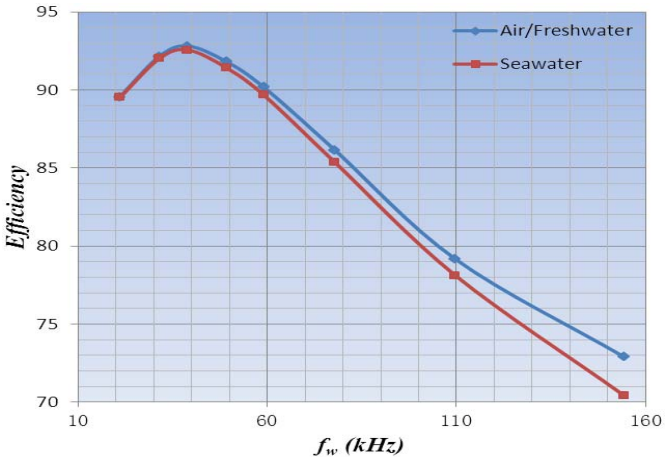

Fig. 16. Transmission efficiency curves of LCT versus operating frequency. IPT system operates at the resonant frequency and at the input voltage of 90 V.

TABLE VI
EXPERIMENTAL RESULTS OF TRANSMISSION EFFICIENCY

f_w (kHz)	C_p (μF)	C_s (μF)	η_{air} (%)	$\eta_{freshwater}$ (%)	$\eta_{seawater}$ (%)
21.0	0.33	0.33	89.565	89.559	89.523
30.1	0.15	0.15	92.146	92.137	92.014
38.9	0.10	0.10	92.818	92.801	92.564
49.1	0.055	0.055	91.826	91.429	91.509
59.0	0.035	0.035	90.185	90.168	89.684
77.8	0.02	0.02	86.160	86.009	85.379
109.7	0.01	0.01	79.167	78.957	78.124
154.2	0.005	0.005	72.921	72.796	70.45

Note - The seawater is prepared under the condition of salinity of 20‰ and 20°C in the experiment. And the operating frequency is not the resonant frequency but the frequency of maximal efficiency.

the actual measured AEC loss with the frequency change is in agreement with that of the calculated loss. However, the measured loss is lower than the calculated loss since the actual core shell is immerged in seawater in the FEM, where the conductivity is greater than that in the actual situation.

Ensuring that the operating frequency is kept at 21 kHz, and the dc bus voltage is increased to increase the primary current. The experimental curve of AEC loss versus primary current is obtained, as shown in Fig. 15. In addition, the simulation curve is shown to compare with the measured result. It can be seen that the trend of the measured AEC loss with the primary current change is in agreement with that of the calculated loss. However, the actual measured loss is much lower than the calculated loss for the same reason above.

For the actual measurement of the winding loss, the RLC tester is used to acquire the winding resistance. Here, the winding resistance is corrected according to the temperature rise of the winding, namely, $\rho = \rho_0 + \rho_0 \cdot \alpha \cdot \Delta t$, where ρ_0 is the resistivity of copper at 0 °C, α is the temperature coefficient of copper, and Δt is the temperature rise. The approximate of winding loss is calculated using the measured current and the remaining part of the total losses is regarded as the core loss. The winding loss and core loss obtained by the above method are 66 and 5 W, respectively, under the experimental conditions of 38.9 kHz operating frequency and 10 A primary current.

According to Table VI, transmission efficiency curves of LCT with the changed operating frequency are obtained, as shown in Fig. 16. Since the transmission efficiency is almost the same in air and freshwater, only the transmission efficiency curves in seawater and air are plotted. Apparently, the transmission efficiency increases at first then decreases with the increasing frequency. An optimal frequency is around 38.9 kHz through the experimental data. When the system operates at 21 kHz, transmission efficiency of the LCT in the three media is nearly the same, which is in the range of 89.5% ± 0.1%. At the operating frequency from 21 to 38.9 kHz, transmission efficiency shows an increasing trend due to the transfer characteristic of IPT system [28]. In air and freshwater, the winding loss accounts for the largest portion. Skin effect results in the increase of winding resistance with the increase of operating frequency. Thus, the increase of winding loss leads to the reduced transmission efficiency of LCT and the lowest efficiency is 73%. In particular, the AEC loss brings about a faster decline of transmission efficiency in seawater. Due to the rapid increase of the AEC loss with frequency, difference of the transmission efficiency in seawater and air has an increased trend, up to 2.47% at the operating frequency of 154.2 kHz.

Fig. 17 shows the transmission efficiency curves of LCT with the changed primary current at the operating frequency of 20 kHz. Obviously, transmission efficiency of LCT in the three media is nearly the same, which is in the range of 87.8% ± 0.3%. This is because that the winding loss is the main loss at 20 kHz and is almost same in the three media. However, due to the AEC loss, transmission efficiency is lowest in seawater and is highest in air. In summary, transmission efficiency in the three media has no significant difference.

Experimental results of the IPT system which operates at the optimal frequency in seawater are shown in Fig. 18. The dc input voltage is 320 V obtained by the ac 220 V uncontrolled rectifier. From the experimental results, it can

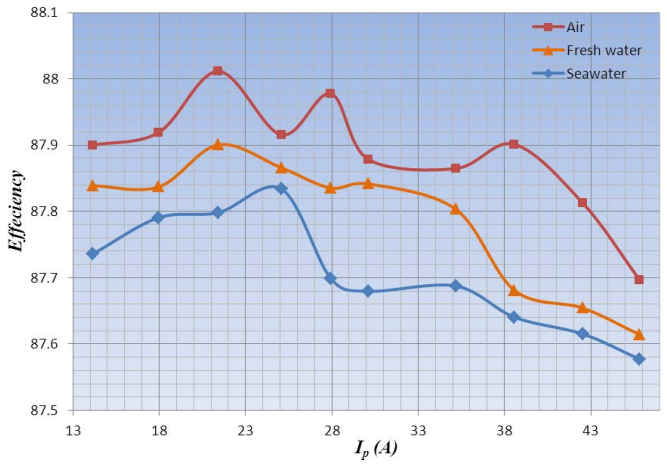

Fig. 17. Transmission efficiency curves of LCT versus primary current ($f_w = 20$ kHz).

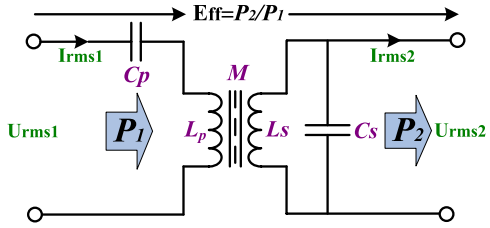

(a)

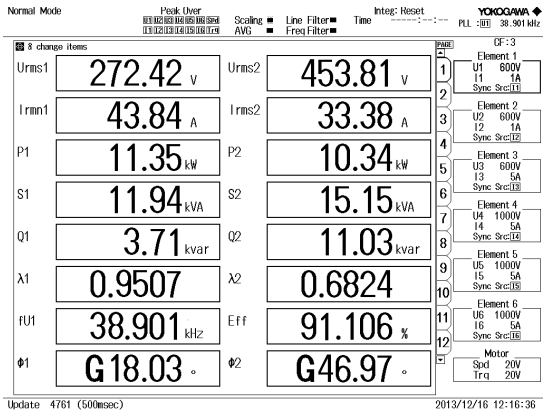

(b)

Fig. 18. Experimental results of 10 kW level IPT system in seawater. (a) Measurement port. (b) Measurement results using power meter.

TABLE VII
LOSS DISTRIBUTION FOR 10 kW SYSTEM

Item	AEC Loss	Winding Loss	Core Loss
Value (W)	514	459	37

be seen that transmission efficiency of the devised LCT is up to 91% when output power of the IPT system is 10 kW. According to the calculation of the three types of loss given in this paper, the breakdown of loss in the 10 kW system [Fig. 18(b)] is shown in Table VII.

VI. CONCLUSION

A novel semiclosed magnetic core structure of underwater LCT is proposed in this paper. This structure is capable of improving the coupling coefficient and reducing the electromagnetic radiation effectively. Given the specificity of water media, power loss of the devised LCT is investigated in three different media, such as air, freshwater, and seawater, comparatively. Simulation results indicate that power loss in air and freshwater are basically identical. Consequently, the freshwater has little effect on the transmission efficiency of LCT. However, in seawater, when operating frequency of the IPT system exceeds a certain value, AEC loss will exceed core loss and winding loss. Furthermore, the AEC loss exerts more and more influence on the transmission efficiency of the IPT system with the operating frequency increasing. The simulation results are verified by the underwater experiment upon an IPT prototype system, which can transfer 10 kW at 91% maximal transmission efficiency. Experimental results show that the transmission efficiency are almost identical in three media at the operating frequency of 21 kHz, while it decreases by 2.5% in seawater compared with the efficiency in freshwater and air at the operating frequency of 154.2 kHz. Therefore, it is suggested that the IPT system for underwater application operate at a low frequency as well as at the frequency of optimal efficiency according to the frequency characteristic curve. Based on the above research, theoretical basis is provided for applications of IPT system on special occasions, such as oceans and lakes.

ACKNOWLEDGMENT

This work is supported in part by National Natural Science Foundation of China under Grant 51277037 and in part by the Scientific Research Foundation of the Higher Education Institutions through Harbin Institute of Technology under Grant 2014018.

REFERENCES

[1] A. P. Hu and S. Hussmann, "Improved power flow control for contactless moving sensor applications," *IEEE Power Electron. Lett.*, vol. 2, no. 4, pp. 135–138, Dec. 2004.
[2] A. Kiefer and L. M. Reindl, "Inductively coupled sensor/actuator system for closed-loop control applications at high temperatures and in aggressive environments," in *Proc. IEEE Sensors*, Oct. 2007, pp. 1396–1399.
[3] K. Tomita, R. Shinoda, T. Kuroda, and H. Ishikuro, "1 W 3.3 V-to-16.3 V boosting wireless power transfer circuits with vector summing power controller," in *Proc. IEEE Asian Solid-State Circuits Conf.*, Nov. 2011, pp. 177–180.
[4] J. L. Villa, J. Sallán, A. Llombart, and J. F. Sanz, "Design of a high frequency inductively coupled power transfer system for electric vehicle battery charge," *Appl. Energy*, vol. 86, no. 3, pp. 355–363, Mar. 2009.
[5] H. H. Wu, G. A. Covic, J. T. Boys, and A. P. Hu, "A 1 kW inductive charging system using AC processing pickups," in *Proc. 6th IEEE Conf. Ind. Electron. Appl.*, Jun. 2011, pp. 1999–2004.
[6] J. Zhou, D.-J. Li, and Y. Chen, "Frequency selection of an inductive contactless power transmission system for ocean observing," *Ocean Eng.*, vol. 60, pp. 175–185, Mar. 2013.
[7] O. H. Stielau and G. A. Covic, "Design of loosely coupled inductive power transfer systems," in *Proc. Int. Conf. Power Syst. Technol. PowerCon*, vol. 1. 2000, pp. 85–90.
[8] T. Misawa, T. Takura, F. Sato, T. Sato, and H. Matsuki, "Parameter design for high-efficiency contactless power transmission under low-impedance load," *IEEE Trans. Magn.*, vol. 49, no. 7, pp. 4164–4167, Jul. 2013.

[9] A. Moradewicz and M. P. Kazmierkowski, "Novel FPGA based control of series resonant converter for contactless power supply," in *Proc. Int. Conf. Comput. Tool EUROCON*, Sep. 2007, pp. 1328–1335.
[10] C.-S. Wang, G. A. Covic, and O. H. Stielau, "General stability criterions for zero phase angle controlled loosely coupled inductive power transfer systems," in *Proc. 27th Annu. Conf. IEEE Ind. Electron. Soc. (IECON)*, vol. 2. 2001, pp. 1049–1054.
[11] U. K. Madawala, M. Neath, and D. J. Thrimawithana, "A power–frequency controller for bidirectional inductive power transfer systems," *IEEE Trans. Ind. Electron.*, vol. 60, no. 1, pp. 310–317, Jan. 2013.
[12] C.-Y. Huang, J. T. Boys, G. A. Covic, and M. Budhia, "Practical considerations for designing IPT system for EV battery charging," in *Proc. IEEE Veh. Power Propuls. Conf.*, Sep. 2009, pp. 402–407.
[13] Y. Kaneko and S. Abe, "Technology trends of wireless power transfer systems for electric vehicle and plug-in hybrid electric vehicle," in *Proc. IEEE 10th Int. Conf. Power Electron. Drive Syst. (PEDS)*, Apr. 2013, pp. 1009–1014.
[14] Z.-S. Li, D. Li, L. Lin, and Y. Chen, "Design considerations for electromagnetic couplers in contactless power transmission systems for deep-sea applications," *J. Zhejiang Univ. Sci. C*, vol. 11, no. 10, pp. 824–834, Sep. 2010.
[15] T. Kojiya, F. Sato, H. Matsuki, and T. Sato, "Automatic power supply system to underwater vehicles utilizing non-contacting technology," in *Proc. Oceans MTTS/IEEE Techno-Ocean*, vol. 4. Nov. 2004, pp. 2341–2345.
[16] H. Fukuda, N. Kobayashi, K. Shizuno, S. Yoshida, M. Tanomura, and Y. Hama, "New concept of an electromagnetic usage for contactless communication and power transmission in the ocean," in *Proc. IEEE Int. Underwater Technol. Symp. (UT)*, Mar. 2013, pp. 1–4.
[17] T. H. Nishimura, T. Eguchi, K. Hirachi, Y. Maejima, K. Kuwana, and M. Saito, "A large air gap flat transformer for a transcutaneous energy transmission system," in *Proc. 25th Annu. IEEE Proc. Power Electron. Specialist Conf. Rec. (PESC)*, vol. 2. Jun. 1994, pp. 1323–1329.
[18] H. Kim, C. Song, J. Kim, J. Kim, and J. Kim, "Shielded coil structure suppressing leakage magnetic field from 100 W-class wireless power transfer system with higher efficiency," in *Proc. IEEE MTT-S Int. Microw. Workshop Ser. Innovative Wireless Power Trans., Technol. Syst. Appl.*, May 2012, pp. 83–86.
[19] A. E. Umenei, J. Schwannecke, S. Velpula, and D. Baarman, "Novel method for selective nonlinear flux guide switching for contactless inductive power transfer," *IEEE Trans. Magn.*, vol. 48, no. 7, pp. 2192–2195, Jul. 2012.
[20] X. Zhang, Y. Zhao, S. L. Ho, and W. N. Fu, "Analysis of wireless power transfer system based on 3-D finite-element method including displacement current," *IEEE Trans. Magn.*, vol. 48, no. 11, pp. 3692–3695, Nov. 2012.
[21] J.-R. Sibue, G. Meunier, J.-P. Ferrieux, J. Roudet, and R. Periot, "Modeling and computation of losses in conductors and magnetic cores of a large air gap transformer dedicated to contactless energy transfer," *IEEE Trans. Magn.*, vol. 49, no. 1, pp. 586–590, Jan. 2013.
[22] G. Bertotti, "General properties of power losses in soft ferromagnetic materials," *IEEE Trans. Magn.*, vol. 24, no. 1, pp. 621–630, Jan. 1988.
[23] N. Kuyvenhoven, C. Dean, J. Melton, J. Schwannecke, and A. E. Umenei, "Development of a foreign object detection and analysis method for wireless power systems," in *Proc. IEEE Symp. Product Compliance Eng. (PSES)*, Oct. 2011, pp. 1–6.
[24] F. Fiorillo, C. Beatrice, O. Bottauscio, and E. Carmi, "Eddy-current losses in Mn-Zn ferrites," *IEEE Trans. Magn.*, vol. 50, no. 1, Jan. 2014, Art. ID 6300109.
[25] Z. Pantic and S. Lukic, "Computationally-efficient, generalized expressions for the proximity-effect in multi-layer, multi-turn tubular coils for wireless power transfer systems," *IEEE Trans. Magn.*, vol. 49, no. 11, pp. 5404–5416, Nov. 2013.
[26] A. van den Bossche, V. C. Valchev, and S. T. Barudov, "Practical wide frequency approach for calculating eddy current losses in transformer windings," in *Proc. IEEE Int. Symp. Ind. Electron.*, vol. 2. Jul. 2006, pp. 1070–1074.
[27] C. R. Sullivan, "Optimal choice for number of strands in a litz-wire transformer winding," *IEEE Trans. Power Electron.*, vol. 14, no. 2, pp. 283–291, Mar. 1999.
[28] S. Hasanzadeh and S. Vaez-Zadeh, "Efficiency analysis of contactless electrical power transmission systems," *Energy Convers. Manage.*, vol. 65, pp. 487–496, Jan. 2013.

Zhiyuan Cheng received the M.S. degree from the Shenyang University of Technology, Shenyang, China, in 2006. He is currently pursuing the Ph.D. degree in instrument science and technology with the Harbin Institute of Technology, Harbin, China.

His current research interests include wireless power transfer and high-power inductive coupling power transfer technologies.

Yang Lei was born in Hubei, China, in 1990. He received the M.Sc. degree in electrical engineering from the Harbin Institute of Technology, Harbin, China, in 2014.

He is currently involved in power system on ships with Harbin Institute of Technology. His current research interests include wireless power transfer, in particular, electromagnetic analysis of the wireless power transfer system.

Kai Song (M'12) received the B.S., M.S., and Ph.D. degrees in instrument science and technology from the Harbin Institute of Technology (HIT), Harbin, China, in 2005, 2007, and 2011, respectively.

He has been a Lecturer with the School of Electrical Engineering and Automation, HIT, since 2011, and a Post-Doctoral Research Fellow with the State Key Laboratory of Robotics and System, HIT, since 2013. He is currently a Visiting Scholar in Electrical Engineering with the University of Tokyo, Tokyo, Japan. His current research interests include wireless power transfer, wireless communication, and advanced sensor technologies.

Chunbo Zhu (M'05) received the B.S. and M.S. degrees in electrical engineering and the Ph.D. degree in mechanical engineering from the Harbin Institute of Technology (HIT), Harbin, China, in 1987, 1992, and 2001, respectively.

He was a Post-Doctoral Research Fellow with the PEI Research Center, National University of Ireland, Galway, Ireland, from 2003 to 2004. He has been a Lecturer with the Department of Automation Measurement and Control, HIT, since 1987. He is currently a Full Professor with HIT, where he leads the Laboratory of Wireless Power Transfer and Battery Management Technologies. His current research interests include energy management systems, electric and hybrid electric vehicles, and wireless power transfer technologies.